Bottlebrush Copolymer Additives for Immiscible Polymer Blends

Hui Zhen Mah, [†‡] Pantea Afzali,[‡] Luqing Qi,[§] Stacy Pesek,[§] Rafael Verduzco,[§*] Gila E. Stein[#*]

[†] Materials Science and Engineering Program, University of Houston, Houston TX 77204; [‡]Department of Chemical and Biomolecular Engineering, University of Houston, Houston TX 77204; [§] Department of Chemical and Biomolecular Engineering, Rice University, Houston TX 77006; # Department of Chemical and Biomolecular Engineering, University of Tennessee, Knoxville TN 37996

ABSTRACT

Thin films of immiscible polymer blends will undergo phase separation into large domains, but this behavior can be suppressed with additives that accumulate and adhere at the polymer/polymer interface. Herein, we describe the phase behavior of polystyrene/poly(methyl methacrylate) (PS/PMMA) blends with 20 vol% of a bottlebrush additive, where the bottlebrush has poly(styrene-r-methyl methacrylate) side chains with 61 mol% styrene. All blends are cast into films and thermally annealed above the glass transition temperature. The phase-separated structures are measured as a function of time with atomic force microscopy and optical microscopy. We demonstrate that subtle changes in bottlebrush architecture and homopolymer chain lengths can have a large impact on phase behavior, domain coarsening, and domain continuity. The bottlebrush additives are miscible with PS under a broad range of conditions, but are only miscible with PMMA when the bottlebrush backbone is short, or when the PMMA chains are similar in length to the bottlebrush side chains. In all other cases, the limited bottlebrush/PMMA miscibility drives the formation of a bottlebrush-rich interphase that encapsulates the PMMA-rich domains, stabilizing the blend against further coarsening at elevated

temperatures. The encapsulated domains are aggregated in short chains or larger networks, depending on the blend composition. Interestingly, the network structures can provide continuity in the minor phases.

INTRODUCTION

Polymer blends can exhibit superior bulk properties than the pure constituents, such as enhanced toughness and impact strength[1,2]. However, most polymer blends will undergo macroscale phase separation[2,3] to generate large and ill-defined domains with weak adhesion at the polymer/polymer phase boundary. Consequently, a phase-separated material will exhibit poor mechanical properties. Surface-active additives such as block polymers[4–9], random copolymers[8,10,11], and polymer-grafted nanoparticles[12–16] will accumulate and adhere at the polymer/polymer interface, thereby dispersing the immiscible polymers into small domains and stabilizing the structures against further coarsening and coalescence. A variety of microstructures can be achieved with proper blend formulation and additive design, including discrete domains or continuous networks with sub-micron length scales[17].

Many polymeric compatiblizers are synthesized from monomers that match the blend constituents. If the blend is comprised of immiscible A and B homopolymers, then copolymers with random or blocky AB sequences can be effective compatibilizers. The copolymer architecture is an important parameter that impacts the surface activity, interfacial strength, and kinetics of structure formation. Long copolymers can form multiple loops between the two phases, which is advantageous for adhesion at the phase boundary[11,18], and they produce a larger reduction in the interfacial tension[8]. Increasing the "blockiness" in a copolymer favors surfactant-like behavior, meaning the additive forms a monolayer at the polymer/polymer interface, while a more random monomer sequence can drive the formation of an interfacial wetting layer[10,18]. Finally, molecular geometry also impacts the interfacial tension: for example, long comb copolymers with many grafted side-chains are more effective compatibilizers than short linear block polymers[8].

Nanoparticle compatibilizers are often coated with polymer brushes that match the chemistry of the parent homopolymers[12]. The objective of these coatings is to generate particles that are evenly wet by the blend constituents, thereby favoring their placement at the A/B interface[12,14,19]. The brushes could be mixtures of A and B homopolymer chains[13,16], AB random copolymer chains[20], or even pure homopolymer chains [15,21]. The architecture of the brush, i.e., areal chain density and chain length, will also impact interfacial activity. Nanoparticle compatibilizers can produce similar blend microstructures as polymeric surfactants, including both discrete domains and co-continuous phases[13,15]. However, the adsorption of nanoparticle compatibilizers at an A/B interface is strong and nearly irreversible, so the microstructure can withstand prolonged high-temperature annealing[13,15] and shear flow[16].

In this study, we report the design of bottlebrush copolymer compatibilizers for immiscible polymer blends. Bottlebrush polymers are architecturally similar to comb polymers, but with a much higher density of side-chains (~1 per backbone monomer)[22] that produce a conformationally-frustrated macromolecule with particulate-like features.[23,24] These materials have shown potential as surface-active additives for polymer melts: as examples, low concentrations of bottlebrush poly(dimethylsiloxane-co-lactic acid) will spontaneously accumulate at the interfaces of linear polylactic acid films[25], and low concentrations of bottlebrush polystyrene will spontaneously accumulate at the interfaces of linear polystyrene films[26]. The latter study proposed that bottlebrush polymer additives are more closely related to polymer-grafted nanoparticles than comb polymers: the highly-branched architecture leads to poor miscibility with long linear polymers[26,27], and there is a strong entropic drive for placement of bottlebrush additives at the free surface and substrate of a thin film[26]. Similar arguments can explain the segregation behaviors of star polymer additives in thin films of block copolymers[28].

Therefore, we expect that bottlebrush additives could rapidly de-mix from a blend, localize at the A/B interface, and inhibit coarsening of the microstructures. The objective of this work is to identify the architectural parameters that enable such behavior.

EXPERIMENTAL METHODS

Materials. All reagents and solvents were purchased from commercially available sources and used as received unless noted. 2,2'-Azobis(2-methylpropionitrile) (AIBN) was purified by recrystallizing in methanol. Inhibitors were removed from styrene and methyl methacrylate monomers using an aluminum oxide column. Dichloromethane was dried with molecular sieves (4 Å). Exo-7-oxabicyclo [2.2.1] hept-5-ene-2,3-dicarboxylic anhydride, norbornene-functionalized chain transfer agent (NB-CTA) and modified Grubbs' catalyst $(H_2IMes)(pyr)_2(Cl)_2RuCHPh$ were synthesized using previously reported methods[29].

Linear Homopolymers. Linear polystyrenes (PS_1 and PS_2) and poly (methyl methacrylates) $PMMA_1$ were purchased from Polymer Source. $PMMA_2$ was synthesized via reversible addition-fragmentation chain-transfer (RAFT) polymerization. $PMMA_3$ was purchased from Agilent Technologies.

Polymer	M_n, kg/mol	N	$Đ$
PS_1	14.8	142	1.03
PS_2	15.9	153	1.01
$PMMA_1$	15.7	157	1.25
$PMMA_2$	13.3	133	1.20
$PMMA_3$	16.7	167	1.04

Table 1: Homopolymer Characterization. M_n is number-average molecular weight, N is degree of polymerization and $Đ$ is dispersity.

Random Copolymer Macromonomer. Linear poly (styrene-r-methyl methacrylate) macromonomers, NB-P(S-r-MMA)-CTA, were synthesized via reversible addition-fragmentation chain-transfer (RAFT) polymerization. S (1.75g, 16.9mmol), MMA (1.7g, 17.0mmol) NB-CTA (117mg, 0.211 mmol) and AIBN (3.53mg, 0.0215mmol) were added into a 25 mL round bottom flask. The solution was purged with nitrogen gas for 30 minutes. The polymerization was initiated by placing the flask in an oil bath at 65°C. After 6 hours, the flask was removed and quenched by immersing in an ice bath. The polymer was then obtained by precipitating in methanol at 4°C and dried under vacuum.

Bottlebrush Random Copolymer (RCBB). Bottlebrush with random copolymer poly (styrene-r-methyl methacrylate) side-chains, hereafter referred to as RC, was prepared by ring-opening metathesis (ROMP) polymerization using the modified Grubbs' catalyst. NB-P(S-r-MMA)-CTA macromonomers were added to a dry, 25 mL round-bottom flask with a stir bar. The flask was then degassed with three pump–purge cycles, and the desired amount of degassed, anhydrous dichloromethane (DCM) was added for a total macromonomer concentration of 0.02–0.05 M. In a separate flask, (H2IMes) $(pyr)_2(Cl)_2$RuCHPh was dissolved in degassed, anhydrous DCM. The catalyst solution was then transferred to the macromonomer-containing reaction flask using a cannula, which initiates the polymerization. The reaction flask was stirred at room temperature for at least 1 hour, and the reaction was then quenched with butyl vinyl ether. The product was collected by precipitation in methanol at 4°C and dried under vacuum at room temperature.

Tg	f_{PS}	N_{sc}	$Đ_{sc}$	N_b	$Đ_b$
$RCBB_1$	0.61	59	1.22	115	2.2
$RCBB_2$	0.61	59	1.20	52	1.4
RC	0.61	59	1.22	---	----

Table 2: Properties of RC and RCBB additives. RC/RCBB side chains have composition f_{PS} (mole fraction styrene), degree of polymerization N_{sc}, and dispersity $Đ_{sc}$. Backbone degree of polymerization and dispersity are N_b and $Đ_b$, respectively.

Instrumentation

Gel Permeation Chromatography (GPC). GPC was performed using a system with an Agilent 1200 module containing three PSS SDV columns in series (100, 1000 and 10000 Å pore sizes), an Agilent variable wavelength UV/vis detector, a Wyatt Technology HELEOS II multiangle laser light scattering (MALLS) detector (λ = 658nm), and a Wyatt Technology Optilab rEX RI detector. This system enables size exclusion chromatography (SEC) with simultaneous refractive index (SEC-RI), UV/vis (SEC-UV/vis) and MALLS detection. The mobile phase used in this system was THF at 40°C with a flow rate of 1 mL/min. Molecular weights and dispersities of linear PS were obtained by conventional calibration with a polystyrene column. In the case of PMMA-containing bottlebrush and linear polymers, the molecular weights were calculated from the dn/dc values measured using a 100% mass recovery method assumption. A detailed explanation of this method is included in Supporting Information.

Nuclear Magnetic Resonance Spectroscopy (NMR). Using a 400 MHz Bruker multinuclear spectrometer, the hydrogen NMR (^{1}H NMR) spectra was obtained in $CDCl_3$ with

tetramethylsilane as an internal standard. Samples with a concentration of 10 mg/mL were placed in 5mm o.d. tubes.

Atomic Force Microscopy (AFM). AFM was performed using a Veeco Dimension 3000 Atomic Force Microscope. The topography and phase contrast were measured through tapping mode. The probes were silicon with an aluminum reflex coating, spring constant of approximately 40 N/m, and resonance frequency of 300 kHz. The parameters used for image acquisition were 1.0 Hz scan frequency, 10 μm x 10 μm and 20 μm x 20 μm scan sizes, and 512 x 512 image resolution. Raw AFM data were processed using the Nanoscope 6.14R1 software from Veeco Instruments. Zeroth-order flattening was used to process both height and phase images. This eliminates any Z offsets formed between scan lines by subtracting each point in the scan line with an average Z value (Z = phase or height).

Contact Angle (CA) Goniometry. The contact angle of DI water on functionalized substrates was measured using a Dataphysics OCA 15EC goniometer. The contact angle measurements were recorded for 60 seconds at 6.25 frames per second from three different areas of the sample. The measurements were then plotted out against a logarithmic time scale, and the equilibrium angle was determined from the observed plateau.

Sample Preparation.

Substrates. Substrates used for all studies were (100)-oriented p-type silicon wafers. Each substrate was rinsed in deionized water to remove dust particles from the surface and dried under a nitrogen stream. Organic contamination was removed with an ultraviolet-ozone cleaner, and a clean oxidized surface was confirmed with measurements of water contact angle (< 5°). A hydroxyl-terminated poly(styrene-r-methyl methacrylate) random copolymer was grafted to the

clean silicon surface to form a "neutral" brush layer, which is intended to screen preferential interactions between PMMA and the underlying substrate.[30,31] The random copolymer was purchased from Polymer Source, and has an M_n = 6.8 kg/mol, Đ = 1.25, and 62 mol% styrene content. The brush was prepared following the protocol described elsewhere[32]. The measured water contact angle of the brush layer ranges from 77-83°.

Polymer Blend Films. The PS/PMMA blend compositions were varied from 45 vol% to 55 vol% with an uncertainty of ±1 vol%. Additives (linear random copolymer or bottlebrush random copolymer) were included in some films at concentrations of 20 wt% relative to the total amount of PS and PMMA. The polymers (PS, PMMA, additives) were dissolved in toluene at a concentration of 3.4-3.6 wt% and the solution was filtered with two 0.2 μm Teflon mesh. Films with thicknesses of 150 nm (± 10 nm) were prepared by spin-casting on the brushed silicon wafers. Thicknesses of as-cast films were measured with a J.A. Woollam M-2000 spectroscopic ellipsometer. The ellipsometry parameters Δ and ψ were modeled by describing the polymer's optical properties with the Cauchy dispersion relation, $n(\lambda) = A + B/\lambda^2$, where λ is the incident wavelength (nm). The optical properties of silicon and native oxide are part of a built-in database. A, B, and film thickness are adjustable parameters for regression analysis. Typical values for A and B are 1.5 and 0.01, respectively. All films were annealed on a hotplate in air (unless stated otherwise) at 150 °C for times ranging from 0 to 85 min.

Selective Removal of PS Domains. PS domains were selectively dissolved from the blend films using cyclohexane. Samples were soaked in cyclohexane for at least 60 seconds and were dried using nitrogen gas.

Image and Domain Size Analysis. The sizes and areas of microstructures were determined by analysis of AFM phase images using ImageJ software. First, the phase images were converted

into an 8-bit grayscale image. Second, the image contrast, brightness, and threshold were adjusted to enhance the areas of interest for analysis. Third, image noise was removed by correcting odd pixels with the median of surrounding pixels using the "remove outliers" function. Last, the perimeter p and area A of the domains were calculated with the built-in particle analysis function. The domain sizes of the microstructures were then calculated by Equation 1[13]:

$$\text{Domain Size} = \pi A/P \quad (1)$$

Where A is the area of the microstructure and P is the perimeter of the microstructure. Histograms of the distribution of the minority domains were based on the area fraction of the minority domains within each range. The area fractions of the minority domains were calculated by dividing the sum of areas of minority domains in each range by the overall areas of the minority domains.

RESULTS AND DISCUSSION

We investigate the effects of bottlebrush copolymer additives on the phase behavior of PS/PMMA blends. Table 1 summarizes the properties of the linear PS and PMMA samples. The bottlebrush copolymer (RCBB) additives are synthesized by a "grafting through" reaction based on ring-opening metathesis polymerization (ROMP) of poly (styrene-r-methyl methacrylate) (PS-r-PMMA) macromonomers with norbornene end groups. This scheme generates one PS-r-PMMA side-chain per backbone norbornene. To test for enthalpic effects, we also examined PS/PMMA blends with PS-r-PMMA macromonomers (RC), i.e., a linear additive with the same length as bottlebrush side chains. The characteristics of all copolymer additives are summarized in Table 2.

All PS/PMMA blend films were prepared with no additive, 12 vol% and 20 vol% of $RCBB_1$, or 20 vol% of RC. The use of films rather than bulk samples allows us to distinguish between PS, PMMA, and RC/RCBB additives through AFM phase imaging[25–27]. PMMA-rich domains are the "brightest" phase in the measurements, PS-rich is the darkest, and RC-rich/RCBB-rich structures generate intermediate contrast. A commonly encountered complication with thin film blends is vertical stratification of constituents due to surface and substrate attraction[33]. PS and PMMA have very similar surface tensions[34], but PMMA is strongly adsorbed at a silicon substrate. Therefore, silicon substrates were coated with a "neutral" PS-r-PMMA brush to suppress adsorption of PMMA at the native oxide[31].

All as-cast films exhibited bumps at the free surface that are approximately 0.5 μm in diameter and 80 nm tall (Figure S1). These protrusions are assigned to a PMMA-rich phase based on the imaging contrast. Such structures are routinely observed in thin film PS/PMMA blends when PS is more soluble in the casting solvent than PMMA[31,35], and are explained by the relative drying rates of each phase[35]: During spin-casting, PMMA is more rapidly depleted of toluene and will "harden" while PS remains swollen. As the PS phase dries, it collapses around the PMMA-rich domains and generates the high-curvature topography. This initial state is highly non-equilibrium, so subsequent annealing above the glass transition (of PS, PMMA, and additives) drives changes in film topography and activates further phase separation. The microstructures that evolve depend on the blend composition and the type of additive.

We checked for through-film uniformity of annealed microstructures by washing away PS in cyclohexane (Figure S2) and found that AFM measurements of the surface are representative of the through-film morphology when the molecular weights of PS and PMMA homopolymers are low ($PS_1/PMMA_1$, $PS_1/PMMA_2$). As discussed in the Supporting

Information, blends with higher molecular weight homopolymers (PS_2/$PMMA_3$) produce structures that are non-uniform with depth into the film (Figures S4-S5), where the PMMA-rich domains are larger near the substrate compared with the surface.

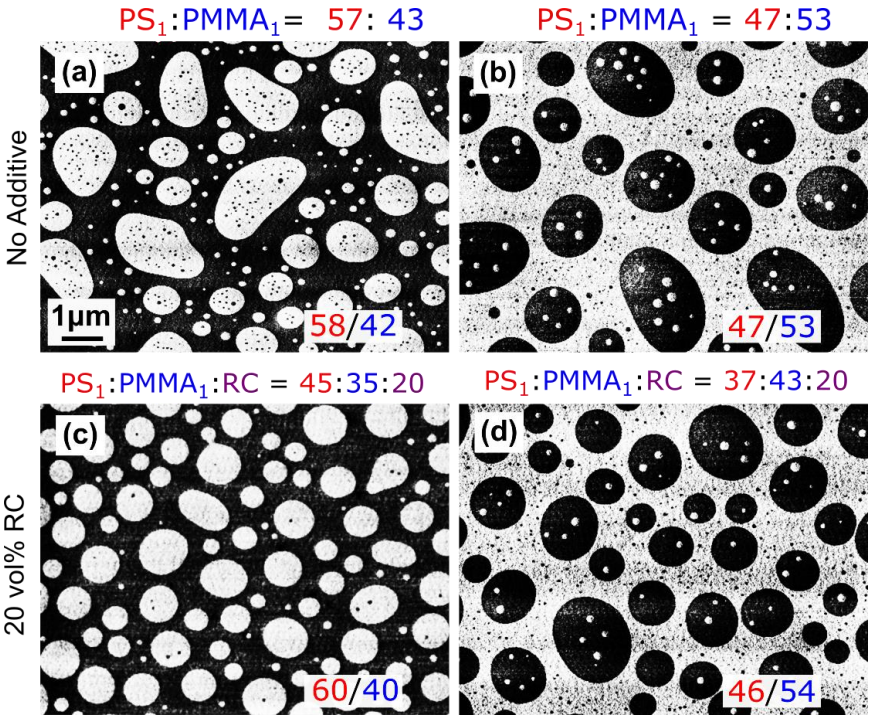

Figure 1. AFM phase images of PS_1 /$PMMA_1$ blend microstructures annealed for 85min, with (a,b) no additive; (c,d) RC additive. The proportion of PS_1:$PMMA_1$ is constant in each column (left: 57:43, right: 47:53). Relative volumes of blend constituents are noted above each micrograph, and the measured relative areas of α:β or α:β:γ phases are marked in the bottom-right of each image. The contrast of α, β, and γ phases are dark, bright, and intermediate, respectively.

Figures 1a and 1b report the microstructure of PS_1/$PMMA_1$ blends having PS volume fractions of Φ_{PS} = 0.57 and 0.47. Using Flory-Huggins theory[2,3,36], we estimate that the majority phase will switch from PS-rich to PMMA-rich at $\Phi_{PS} \approx 0.5$ (see Supporting Information). After 85 min of annealing, the outcomes of PS_1/$PMMA_1$ are as-expected: blends with $\Phi_{PS} > 0.5$ phase-separate into a PS-rich matrix with PMMA-rich minority domains, while blends with $\Phi_{PS} < 0.5$ exhibit the inverse structure. We then consider the effects of RC linear additive on PS_1/$PMMA_1$ blends. The proportion of PS_1:$PMMA_1$ remains the same, i.e., 57:43 and 47:53 vol:vol, but the

overall composition is changed by the addition of 20 vol% RC. As observed in Fig. 1c and 1d, the RC additive reduces the size of the of minority domains and increases their circularity, but the microstructures are otherwise very similar to blends with no additive. Figure S6 reports the size distribution of minority domains for each proportion of PS_1:$PMMA_1$ with and without RC additive.

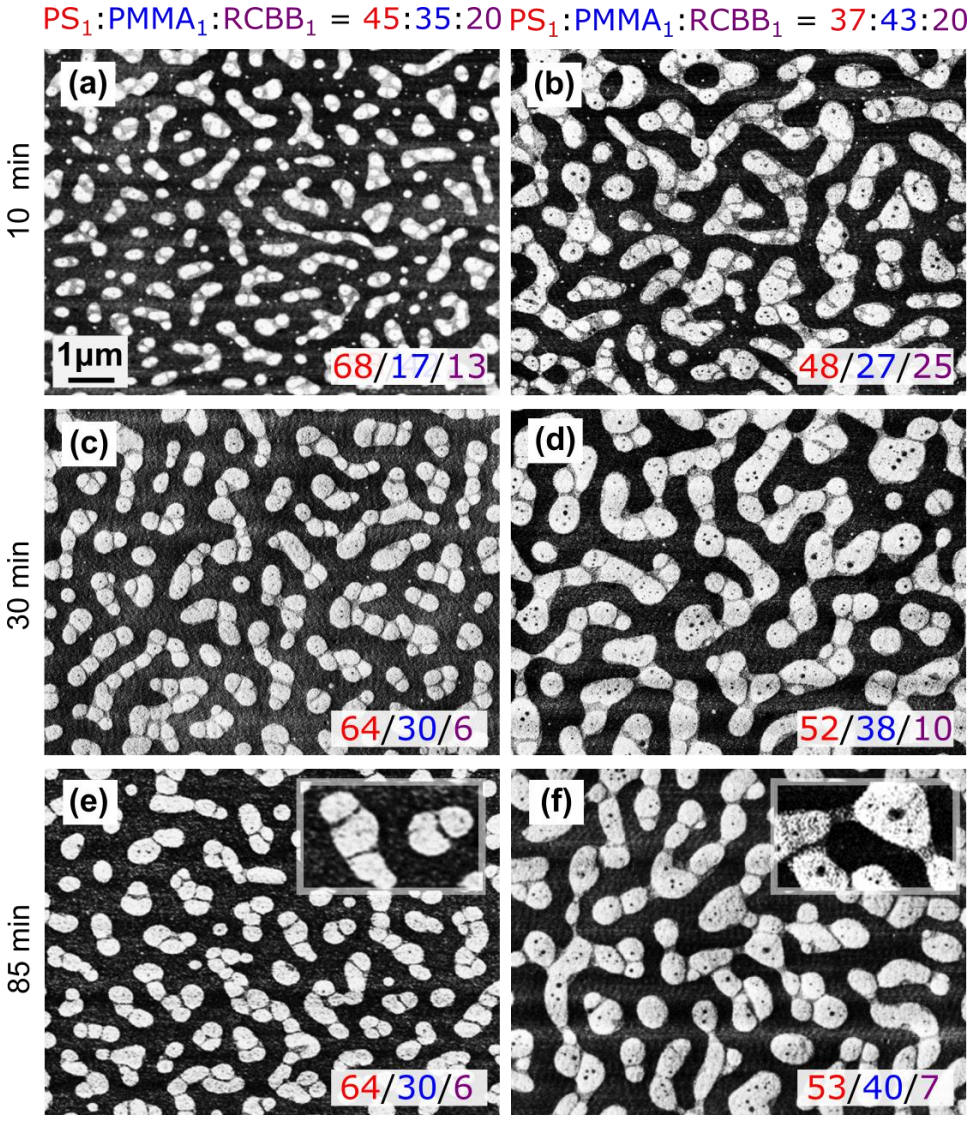

Figure 2. AFM phase images of PS_1/$PMMA_1$ blends with 20 vol% of $RCBB_1$ additive. (a,b) 10 min; (c,d) 30 min; and (e,f) 85 min, inset at twice the magnification. Relative volume of PS_1/$PMMA_1$ blend constituents is fixed in each column (left: 57:43, right: 46:54), and relative volumes of α:β or α:β:γ phases are marked in the bottom-right of each image. The contrast of α, β, and γ phases are dark, bright, and intermediate, respectively.

The effects of bottlebrush $RCBB_1$ additive on the PS_1/$PMMA_1$ blends (57:43 and 47:53) are reported in Figure 2 as a function of annealing time; 2e and 2f show data for 85 min, which is the same annealing time that is shown in Figure 1. There are two clear changes in the phase-separated structure: First, both blend compositions show a PS-rich majority phase, which demonstrates that $RCBB_1$ additive is not evenly distributed between PS_1 and $PMMA_1$. Second, the $RCBB_1$ additive drives the formation of a three-phase system. The microstructure in these cases resembles chains of small, circular PMMA-rich domains encapsulated by a RCBB-rich interphase.

The composition of each phase was estimated through image analysis and mass balances. First, the areas of PS-rich (α), PMMA-rich (β), and bottlebrush-rich (γ) phases were calculated from the AFM phase images. These microstructures are uniform with depth (Figure S2), so the area fraction of each phase at the surface is equal to the bulk volume fraction (V). The volume fractions of each phase are reported at the bottom-right of each micrograph in Figure 1. Second, the total amount of PS, PMMA, and additive in each blend are known, so the composition of each phase can be determined from a mass balance[31]. The general form of this mass balance for a two-phase system is

(2) $\Phi_{PX} = \varphi_{PX}^{\alpha} V^{\alpha} + \varphi_{PX}^{\beta} V^{\beta}$,

and for a three-phase system is

(3) $\Phi_{PX} = \varphi_{PX}^{\alpha} V^{\alpha} + \varphi_{PX}^{\beta} V^{\beta} + \varphi_{PX}^{\gamma} V^{\gamma}$.

In equations (2) and (3), the symbol "*PX*" designates the type of polymer, such as PS_1, $PMMA_1$, RC, $RCBB_1$, etc. The parameters φ_{PX}^{i} are the volume fractions of polymer "*PX*" in phase "*i*" and are determined by solving the system of linear equations.

For the binary PS_1/$PMMA_1$ blends, we estimate $\varphi_{PS}^{\alpha} = 0.95$ and $\varphi_{PS}^{\beta} = 0.04$. These values are consistent with predictions from Flory-Huggins theory (Supporting Information), which offers validation for the mass balance approach and suggests that the blend compositions are equilibrated. The compositions of each phase in the ternary PS_1/$PMMA_1$/RC blend are summarized in Table 3. These data demonstrate that RC additive with f_{PS} = 0.61 is miscible with both homopolymers up to at least 20% by volume. The estimated compositions of each phase in the ternary PS_1/$PMMA_1$/$RCBB_1$ blends are summarized in Table 4. The estimated compositions of the PMMA-rich and bottlebrush-rich phases are reported with large uncertainties, as there are degeneracies when fitting a large number of parameters to a limited data set. However, we determined that $RCBB_1$ is partially miscible with PS_1, but limited miscibility with $PMMA_1$ drives the formation of a bottlebrush-rich γ phase.

The limited miscibility between $RCBB_1$ additive and $PMMA_1$ could arise from enthalpic incompatibility between these constituents, entropic factors due to the highly branched bottlebrush architecture, or both effects. With regards to enthalpic interactions, the linear RC additive has the same styrene composition as $RCBB_1$ (f_{PS} = 0.61) and is equally soluble in both PS_1 and $PMMA_1$ up to 20 vol% (Table 3, Figure 1). It is important to note that the RC additive is the same molecular weight as the $RCBB_1$ side chains, meaning the overall size of the bottlebrush additive is much larger than the linear additive, so this control experiment does not cleanly separate the role of enthalpic interactions from the entropic effects of architecture and molecular weight. Furthermore, the bottlebrush/linear interface is characterized by a high density of side-

chain end groups (dodecyl, from the RAFT chain transfer agent), so the unusual architecture could magnify the effects of end-group compatibility with each homopolymer.[37] Therefore, we examine the roles of enthalpic interactions by synthesizing a series of bottlebrush random copolymers with short backbones, and examine their miscibility in PS/PMMA blends. The outcomes are reported in the Supplemental Information (Figure S14). These data suggest that dodecyl-terminated bottlebrushes with $f_{PS} \sim 0.5$ have near-equal solubility in PS and PMMA. While this result may seem intuitive, the miscibility of linear poly(styrene-r-methyl methacrylate) in PMMA and PS has been examined by others,[38,39] and these studies demonstrate that S-rich poly(styrene-r-methyl methacrylate) copolymers are more soluble in PMMA than PS.

Entropic factors can strongly influence the miscibility of architecturally-complex polymer blends. Prior studies have shown that the miscibility of bottlebrush and linear polymer architectures is partly controlled by backbone and side chain conformational entropy. In the absence of enthalpic interactions, short linear chains can swell a long bottlebrush additive and promote backbone extension, while long linear chains drive bottlebrush contraction to an ideal coil.[27] It has also been proposed that short linear chains can penetrate and "wet" the bottlebrush side-chains,[26] similar to the wetting of linear polymers at "brushy" surfaces,[40] which enables their dispersion in the linear melt. In the present system, the $PMMA_1$ chains are longer than PS_1, and PMMA is slightly stiffer than PS[36], so $PMMA_1$ is a poorer "solvent" for the highly-branched RCBB additive than PS_1. The various roles of bottlebrush architecture on blend compatibility are further elaborated in later sections of this manuscript.

Table 3: Compositions of PS-rich (α) and PMMA-rich (β) phases in PS_1:$PMMA_1$:RC blends, calculated from analysis of V^{α} and V^{β} in 45:35:20 and 37:43:20 blends. 85 min anneal.

PX	$\varphi_{PX}^{\propto}$	φ_{PX}^{β}
PS_1	0.7	0.1
$PMMA_1$	0.1	0.7
RC	0.2	0.2

Table 4: Compositions of PS-rich (α), PMMA-rich (β), and bottlebrush-rich (γ) phases in PS_1:$PMMA_1$:$RCBB_1$ blends, calculated from analysis of V^{α}, V^{β}, and V^{γ} in 45:35:20 and 37:43:20 blends. 85 min annealed.

PX	$\varphi_{PX}^{\propto}$	φ_{PX}^{β}	φ_{PX}^{γ}
PS_1	0.7	0.01-0.02	0.05-0
$PMMA_1$	0.1	0.84-0.92	0.43-0
$RCBB_1$	0.2	0.15-0.06	0.52-1

The time evolution of the PS_1/$PMMA_1$/$RCBB_1$ microstructure is illustrated in Figure 2 for two blend compositions, with the corresponding OM data in Figure S7. The microstructure quickly develops, but there is exchange of material between the three phases at short times. In both blend compositions, the $PMMA_1$-rich β phase grows at the expense of the $RCBB_1$-rich γ phase, consistent with limited miscibility between these constituents. Figure 3 includes a statistical analysis of the PMMA-rich domain size distributions (β phase) as a function of time. Within 30 minutes of annealing, the microstructures are resistant to further coarsening, which demonstrates that the bottlebrush-rich γ phase creates a strong encapsulation layer. For comparison, the minority phase in neat blends will coarsen over the same time scales, and these data are summarized in Figure S6.

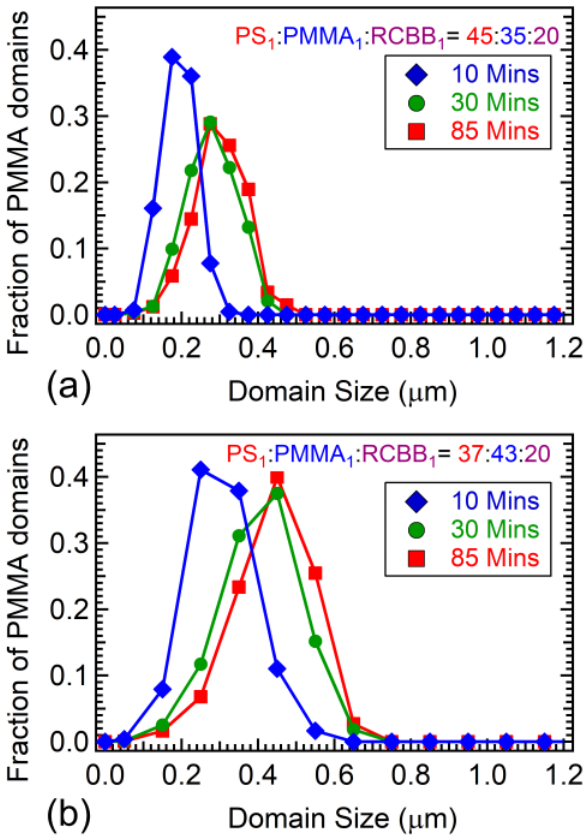

Figure 3. Domain size distributions of β phase in PS_1/$PMMA_1$ with 20 vol% of $RCBB_1$ additive. Relative volume of PS_1:$PMMA_1$ blend constituents is fixed at (a) 57:43 and (b) and 47:53.

We also investigated the effects of additive loading by preparing a 57:43 PS_1:$PMMA_1$ blend with 12 vol% of $RCBB_1$ additive (PS_1/$PMMA_1$/$RCBB_1$ = 49:39:12), and then compared the results with blends that have same proportions of PS_1:$PMMA_1$ but 20 vol% of $RCBB_1$ additive (PS_1/$PMMA_1$/$RCBB_1$ = 45:35:20). First, we observe a decrease in the average size of the PMMA-rich domains when the RCBB additive loading increases from 12 to 20 vol%. Second, the PMMA-rich domains coarsen over time with 12 vol% additive, while the coarsening is suppressed after 30 mins with 20 vol% additive (Figure 3). These behaviors are attributed to a thicker interphase with higher RCBB loading[13,16]: as shown in Figure 4a, with 12 vol% additive, the interfacial layer is not observed in all regions.

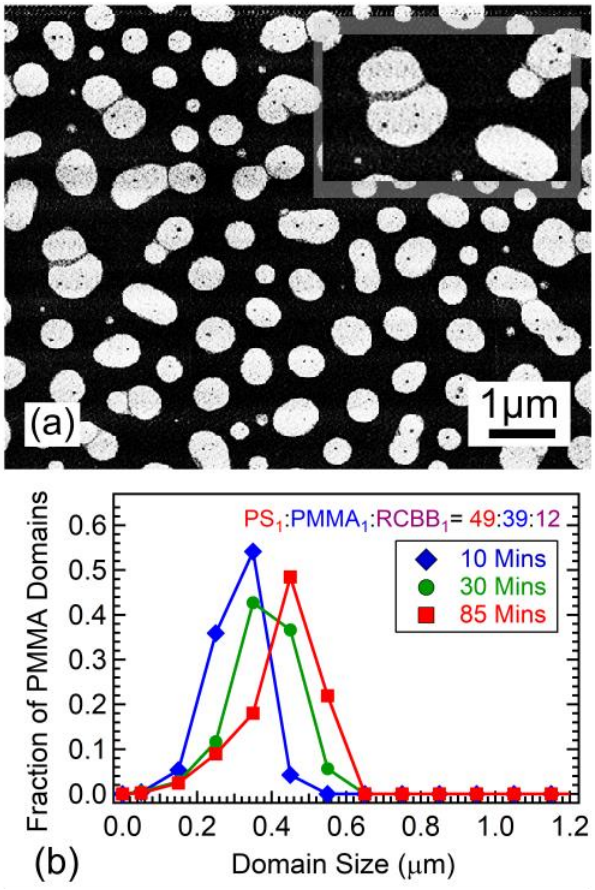

Figure 4: (a) AFM phase image of 57: 43 $PS_1/PMMA_1$ blends with 12 vol% of $RCBB_1$ additive annealed for 85 mins and (b) time evolution of domain size distribution.

As previously discussed, the formation of an encapsulation layer in $PS_1/PMMA_1/RCBB_1$ blends might be attributed to an entropy-controlled de-mixing of $PMMA_1$ and $RCBB_1$. To test this point, we prepared ternary blends using $PS_1/PMMA_2/RCBB_1$. $PMMA_2$ is a slightly lower molecular weight than $PMMA_1$, and may therefore be a better "solvent" for the RCBB additive.[26,27] If the $RCBB_1$ additive is evenly partitioned between the two phases, then we expect a transition from a PS-rich to PMMA-rich majority phase near $\Phi_{,PS} \approx 0.5$. Ternary blends were prepared with 20 vol% of $RCBB_1$ additive and PS_1:$PMMA_2$ volume ratios of 57:43, 52:48, and

47:53. Figure 5 reports AFM phase images for the latter two blend compositions as a function of time. Figures S8-S9 includes additional AFM and OM data for all blends.

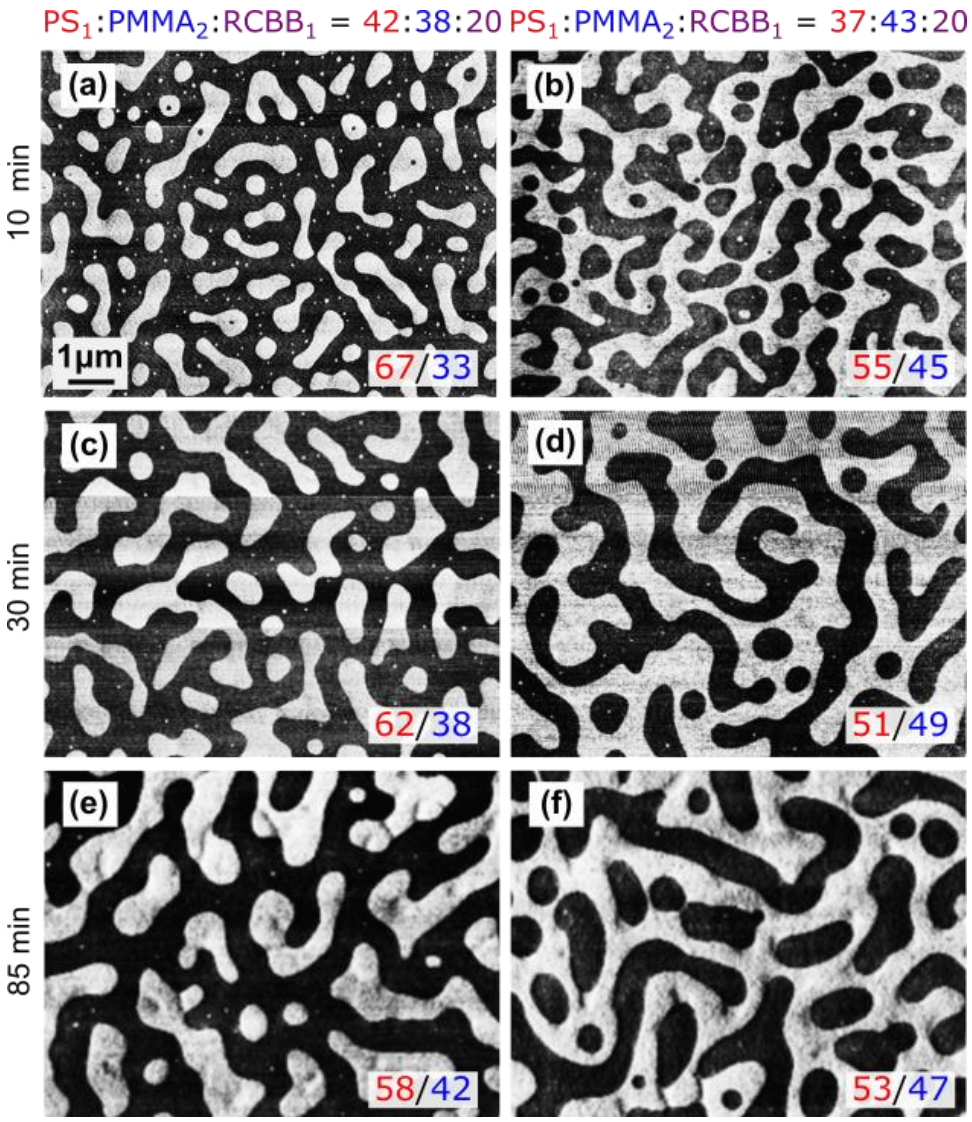

Figure 5. AFM phase images of PS_1/$PMMA_2$ blends with 20 vol% $RCBB_1$ additive. (a,b) 10 min; (c,d) 30 min; and (e,f) 85 min. The α, β, and γ phases are dark, bright, and intermediate contrast, respectively. Relative volume of blend constituents is fixed in each column (left: 52:48, right: 47:53), and relative volumes of α:β phases are marked in the bottom-right of each image.

Upon annealing, the PS_1/$PMMA_2$/RCBB blends form two phases, PS-rich (α) and PMMA-rich (β). Through qualitative inspection and quantitative analysis of the AFM micrographs, we conclude that the $RCBB_1$ additive is soluble in both PS_1 and $PMMA_2$: First,

there is no sign of an encapsulation layer at any annealing time. Second, the structure "inverts" near the expected $\Phi_{,PS} \approx 0.5$ for a neat blend: a PS-rich majority phase is observed when the ratio of PS_1:$PMMA_2$ is 57:43 (Figure S8-S9) and 52:48 (Figure 5a,c,e), while a PMMA-rich majority phase is observed for the 47:53 ratio (Figure 5b,d,f). Finally, through image analysis and mass balances, we find that bottlebrush is equally soluble in the α and β phases. The calculated composition of each phase after 85 min of annealing is reported in Table 5. These outcomes support the hypothesis that entropic effects associated with wetting at the bottlebrush/linear interface are partly controlling the miscibility of the bottlebrush and PMMA constituents. The transition from a state of complete to partial miscibility occurs when the linear PMMA chains are 2.5-3 times longer than the bottlebrush side chains, which is consistent with a prior study of bottlebrush/linear polystyrene blends,[26] and similar to predictions for homopolymer/brush wetting at low curvature surfaces.[40]

Table 5: Compositions of PS-rich (α) and PMMA-rich (β) phases in PS_1/$PMMA_2$:RCBB blends, calculated from analysis of V^{α}, V^{β}, and V^{γ} in 45:35:20, 42:38:20, and 37:43:20 blends. 85 min anneal.

PX	$\varphi_{PX}^{\propto}$	φ_{PX}^{β}
PS_1	0.7	~ 0
$PMMA_2$	0.1	0.8
$RCBB_1$	0.2	0.2

The microstructure in PS_1/$PMMA_2$/RCBB blends is distinct from neat blends or blends with RC additive: small, circular minority domains are aggregated in longer chains, much like the PS_1/$PMMA_1$/$RCBB_1$ system. This suggests that some $RCBB_1$ additive accumulates at the PS_1/$PMMA_2$ interface during the early stages of annealing, perhaps a monolayer (or less) that cannot be detected with AFM. However, a thin surfactant-like layer cannot stabilize the microstructure against coarsening. Through visual inspection of Figure 4, we see that minority

domains in the blend are growing over the time scale of the experiment, which is confirmed by the complete statistical analysis in Figure 6. Figure 6a reports the size distribution of PMMA-rich domains (β phase) for a blend composition of 52:48 PS_1:$PMMA_2$. Figure 6b reports the size distribution of PS-rich domains (α phase) for a blend composition of 47:53 PS_1:$PMMA_2$, as the PMMA-rich domains form a continuous matrix.

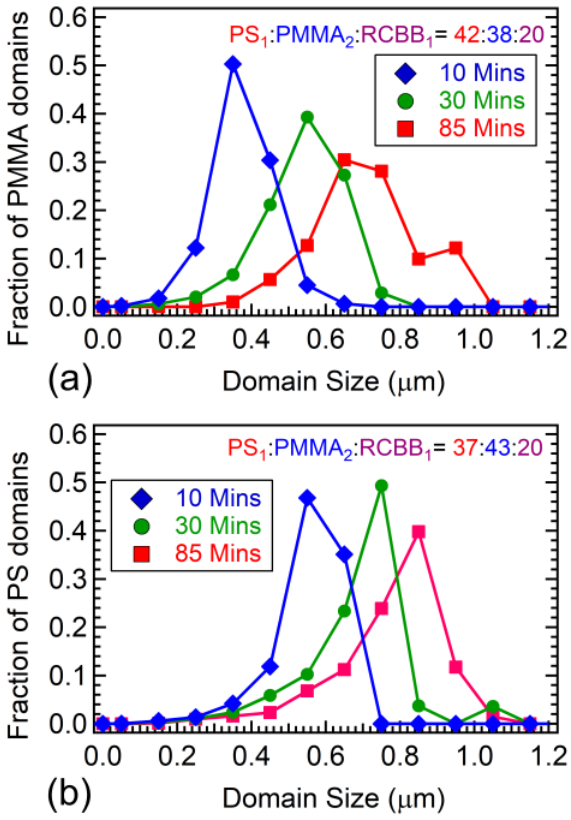

Figure 6. Domain size distributions of PS_1/$PMMA_2$ with 20 vol% of RCBB additive. Relative volume of PS_1/$PMMA_2$ blend constituents is fixed at (a) 52:48 and (b) 47:53

To further illustrate the formation and function of RCBB encapsulation layers, we prepared ternary blends of PS_2/$PMMA_3$/$RCBB_1$. Both PS_2 and $PMMA_3$ have higher molecular weights than all other PS and PMMA blend constituents (PS_1, $PMMA_1$, $PMMA_2$). As with the other blends, if the bottlebrush is evenly partitioned between the two homopolymers, then we anticipate a transition from PS-rich to PMMA-rich majority phase when $\Phi_{PS} \approx 0.5$. Ternary

blends of PS_2/$PMMA_3$ with 20 vol% of $RCBB_1$ additive were prepared with PS_2/$PMMA_3$ volume ratios of 57:43, 52:48 and 47:53. Figures 7a and 7b reports the AFM images for the latter two blends compositions; the microstructures in 57:43 blends were highly non-uniform across different regions, as shown in Figure S11.

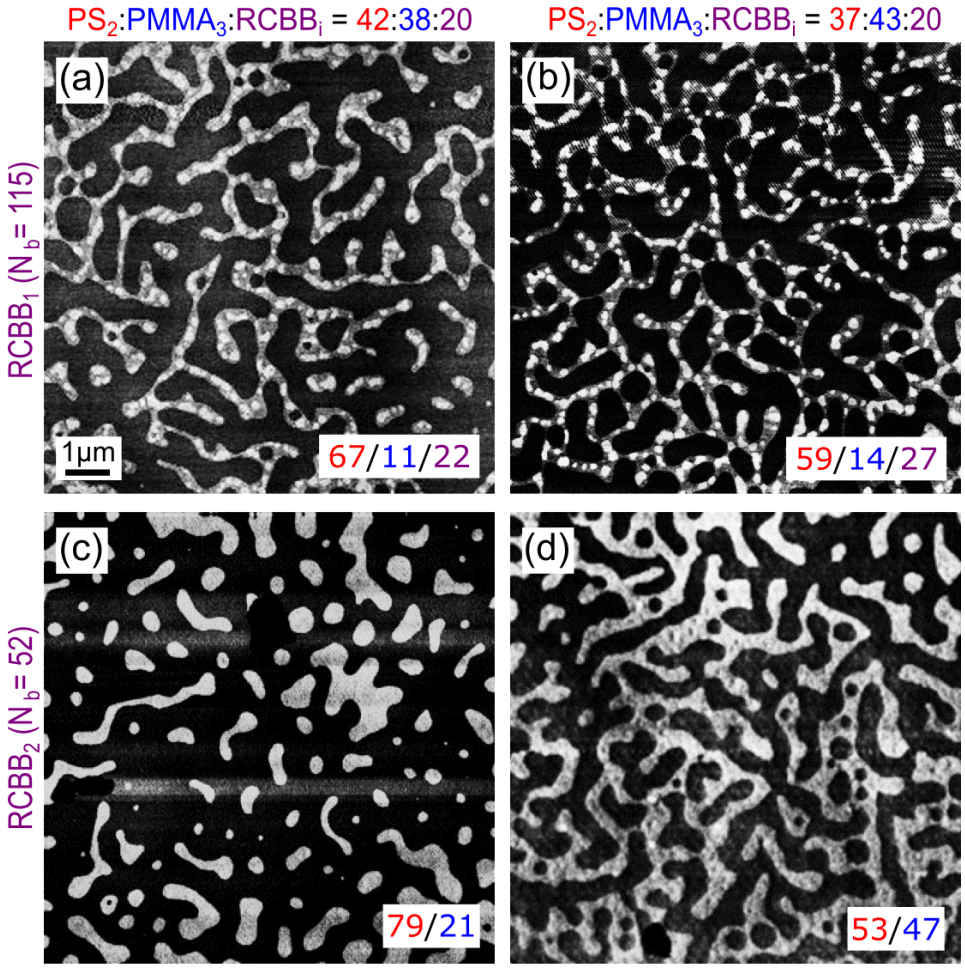

Figure 7: AFM phase images of PS_2/$PMMA_3$ blends with 20 vol% of RCBB additives of different backbone lengths and annealed for 85 min. The proportion of PS_2/$PMMA_3$ in blends are (a, c) 52:48 and (b, d) 47:53. The backbone length of the RCBB additives is fixed in each row (top: N_b=115, bottom: N_b = 52), Relative volumes of the blend constituents are noted in on the left side of the micrograph, and the relative volumes of α:β or α:β:γ phases are marked in the bottom-right of each image. The contrast of α, β, and γ phases are dark, bright, and intermediate, respectively.

From the AFM images, we observe a three-phase system, i.e. a PS-rich α phase, a PMMA-rich β phase and a RCBB-rich γ phase. Based on the previous analysis of the PS/PMMA

systems, we expect the $RCBB_1$ additive to have very limited miscibility in the higher molecular weight PMMA phase (β phase), but it is unclear if increasing the length of the PS chains will reduce bottlebrush/PS miscibility. We do not apply mass balances to this blend system, as the domain sizes are not uniform throughout the film thickness: the widths of the PMMA/RCBB features increase with depth into the film, a sign of preferential wetting by PS at the free surface and/or PMMA at the substrate (Figure S4-S5). However, we offer a few qualitative observations based on the area fraction of each phase at the surface: First, as in the other blends, a PS-majority phase is observed when $\Phi_{PS} < 0.5$, which suggests that $RCBB_1$ remains soluble in PS as molecular weights are increased. Second, the interphase is considerably more diffuse, and its area fraction (at the surface) exceeds the volume fraction of $RCBB_1$ in the blend. This may reflect a greater surface attraction for the branched additive compared with a long linear polymer.[26,41,42] Finally, we note that the interphase is continuous throughout the plane of the film in Figure 7b (PS_2:$PMMA_3$ = 47:53), despite the relatively low concentration of $RCBB_1$ in the blend. Furthermore, the interphase is nearly continuous in the $PS_1/PMMA_1/RCBB_1$ blends and $PS_2/PMMA_3/RCBB_1$ blends shown in Figure 2b and Figure 7a, respectively, where the proportion of PS in the blend is slightly higher (PS_2:$PMMA_3$ = 52:48). Continuous minority phases are notoriously difficult to achieve in blend systems[43], but have been observed in other studies that employ architecturally-complex compatibilizers[44], albeit with different underlying thermodynamics.

Analysis of the domain sizes in the $PS_2/PMMA_3/RCBB_1$ blends confirms that the encapsulation layer suppresses coalescence of the PMMA-rich domains after 30 mins of annealing. The time evolution of domain sizes is reported in Figure 8 for blends with $PS_2/PMMA_3$ = 57:43 (Figure 8a) and 47:53 (Figure 8b). Note that Figure 8a illustrates the size

distribution of the encapsulated PMMA domains, while Figure 8b reports the size distribution of the PS domains. In Figure 8a, we report the size distribution of PMMA domains with the interphase encapsulation layer because it was difficult to identify the individual PMMA domains. In Figure 8b, we report the size distribution of PS domains because the encapsulated PMMA domains formed a continuous matrix.

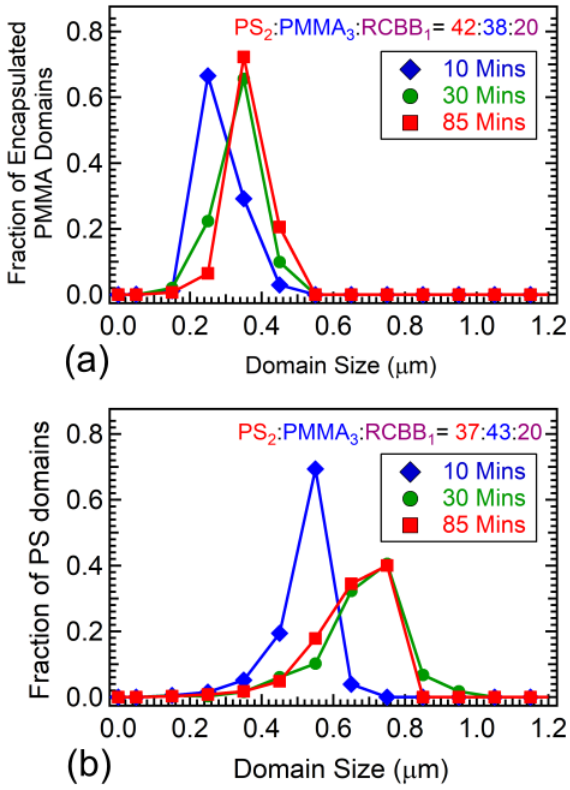

Figure 8: Domain size distributions of PS_2/$PMMA_3$ with 20 vol% of $RCBB_1$ additive. Relative volume of PS_2/$PMMA_3$ blend constituents is fixed at (a) 57:43 and (b) 47:53.

We also studied the effects of the bottlebrush backbone length, N_b, by preparing ternary blends using PS_2 and $PMMA_3$ homopolymers with $RCBB_2$ at volume ratios of 57:43, 52:48, and 47:53. $RCBB_2$ is a random copolymer bottlebrush additive with the same side chain length and

styrene composition as $RCBB_1$, but with a shorter backbone length, i.e., $N_b = 52$ instead of $N_b = 115$. The different backbone length changes the overall size of the additive as well as the aspect ratio. We then compared this system to the same blend compositions with 20 vol% $RCBB_1$. Outcomes are reported in Figure 7. Additional AFM images and OM images for this study are included in Supporting Information.

From the AFM results, we observe a transition from a three-phase system to a two-phase system for all $PS_2/PMMA_3$ blend compositions as the backbone length of the RCBB additive decreases. Considering that the volume of the PMMA-rich phase increases as backbone length is reduced, we conclude that miscibility with PMMA is enhanced by this change to the bottlebrush architecture. As the chemistry of the bottlebrush is unchanged, this enhancement is due to a gain in the configurational entropy of mixing. In the context of a Flory-type model for architecturally-complex blends, the bottlebrush is viewed as a linear polymer with degree of polymerization N_b and monomer size

CONCLUSIONS

We examined the effects of bottlebrush P(S-r-MMA) additives on the phase behavior of PS/PMMA polymer blends in thin films. The bottlebrush side chain length and composition are fixed at N_{sc} = 59 and 61 mol% styrene, respectively, and the bottlebrush concentration in the blends is 20 vol%. We demonstrate that subtle changes in bottlebrush architecture and homopolymer chain lengths can have a large impact on phase behavior, domain coarsening, and domain continuity. The bottlebrush copolymer additives are miscible with PS under all the conditions we studied, which is contrary to prior studies with linear copolymer architectures (60

mol% styrene) that report greater miscibility with PMMA.[39] This discrepancy might be a consequence of the dodecyl-terminated chain ends at the bottlebrush/PS interface, but further studies with different end groups are needed to clarify such effects. In contrast, bottlebrush miscibility with PMMA is a function of the overall bottlebrush size and the relative length of PMMA chains to bottlebrush side chains. When the bottlebrush backbone is short (N_b = 52), and/or the PMMA homopolymer chain lengths are short (N = 133), the bottlebrush additives are equally miscible with both PS and PMMA. Therefore, the phase separation process is largely controlled by immiscibility between PS and PMMA, and the resulting structure is comprised of PS-rich and PMMA-rich domains that coarsen with time. However, by increasing the length of the bottlebrush backbone (115 branches) and the PMMA homopolymer ($N \geq 146$), the bottlebrush/PMMA miscibility is reduced. As a result, the system separates into three-phases: PS-rich, PMMA-rich, and a bottlebrush-rich interphase. We suggest that bottlebrush/PMMA miscibility is largely controlled by 1) conformational entropy of side chains, which is tied to wetting at the brush/linear interface; and 2) the configurational entropy of mixing, which is controlled by the overall sizes of bottlebrushes and linear polymers. Significantly, under conditions that produce three phases, the bottlebrush-rich interphase encapsulates the PMMA-rich domains and suppresses their coarsening at elevated temperatures. Furthermore, the encapsulated PMMA-rich domains are aggregated into longer strings, and the blend composition can be tuned to produce continuity in this microstructure. Bottlebrush additives offer a few unique attributes that could be useful for fundamental studies of soft, brushy nanoparticles, as well as select applications: they are entirely organic, their aspect ratio and composition is easily tuned through synthesis, and they do not entangle during processing.

ASSOCIATED CONTENT

Supporting Information.

Additional studies involving a bottlebrush copolymer with a mixture of PS and PMMA side chains, additional studies with random copolymer side chains having different styrene compositions, additional studies with mixed side chains, and details that pertain to image analysis and mass balances. This material is available free of charge via the Internet at http://pubs.acs.org.

AUTHOR INFORMATION

Corresponding Author

* gstein4@utk.edu; rafaelv@rice.edu

Author Contributions

The manuscript was written through contributions of all authors. All authors have given approval to the final version of the manuscript.

Notes

The authors declare no competing financial interests.

ACKNOWLEDGMENT

H.Z. Mah and G.E. Stein acknowledge financial support from the National Science Foundation under Grant No. DMR-1151468 and CMMI- 1740457. P. Afzali acknowledges financial support from the UH SURF and PURS programs, and an REU supplement from the National Science Foundation under Grant No. DMR-1151468. L. Qi, S.L. Pesek, and R. Verduzco acknowledge financial support from the National Science Foundation under Grant No. CMMI-1563008 and the Welch Foundation for Chemical Research under Grant No. C-1888.

REFERENCES

(1) Robeson, L. Historical Perspective of Advances in the Science and Technology of Polymer Blends. *Polymers* **2014**, *6* (5), 1251–1265.

(2) Robeson, L. M. *Polymer Blends: A Comprehensive Review*; Hanser: Munich, 2007.

(3) Eitouni, H. B.; Balsara, N. P. Thermodynamics of Polymer Blends. In *Physical Properties of Polymers Handbook*; Mark, J. E., Ed.; Springer New York, 2007; pp 339–356.

(4) Fredrickson, G. H.; Bates, F. S. Design of Bicontinuous Polymeric Microemulsions. *J. Polym. Sci. Part B Polym. Phys.* **1997**, *35* (17), 2775–2786.

(5) Anderson, K. S.; Hillmyer, M. A. The Influence of Block Copolymer Microstructure on the Toughness of Compatibilized Polylactide/Polyethylene Blends. *Polymer* **2004**, *45* (26), 8809–8823.

(6) Galloway, J. A.; Jeon, H. K.; Bell, J. R.; Macosko, C. W. Block Copolymer Compatibilization of Cocontinuous Polymer Blends. *Polymer* **2005**, *46* (1), 183–191.

(7) Lyatskaya, Y.; Gersappe, D.; Balazs, A. C. Effect of Copolymer Architecture on the Efficiency of Compatibilizers. *Macromolecules* **1995**, *28* (18), 6278–6283.

(8) Lyatskaya, Y.; Gersappe, D.; Gross, N. A.; Balazs, A. C. Designing Compatibilizers To Reduce Interfacial Tension in Polymer Blends. *J. Phys. Chem.* **1996**, *100* (5), 1449–1458.

(9) Shull, K. R.; Kellock, A. J.; Deline, V. R.; MacDonald, S. A. Vanishing Interfacial Tension in an Immiscible Polymer Blend. *J. Chem. Phys.* **1992**, *97* (3), 2095–2104.

(10) Lefebvre, M. D.; Dettmer, C. M.; McSwain, R. L.; Xu, C.; Davila, J. R.; Composto, R. J.; Nguyen, S. T.; Shull, K. R. Effect of Sequence Distribution on Copolymer Interfacial Activity. *Macromolecules* **2005**, *38* (25), 10494–10502.

(11) Eastwood, E. A.; Dadmun, M. D. Multiblock Copolymers in the Compatibilization of Polystyrene and Poly(Methyl Methacrylate) Blends: Role of Polymer Architecture. *Macromolecules* **2002**, *35* (13), 5069–5077.

(12) Ku, K. H.; Yang, H.; Jang, S. G.; Bang, J.; Kim, B. J. Tailoring Block Copolymer and Polymer Blend Morphology Using Nanoparticle Surfactants. *J. Polym. Sci. Part Polym. Chem.* **2015**, n/a-n/a.

(13) Bryson, K. C.; Löbling, T. I.; Müller, A. H. E.; Russell, T. P.; Hayward, R. C. Using Janus Nanoparticles To Trap Polymer Blend Morphologies during Solvent-Evaporation-Induced Demixing. *Macromolecules* **2015**.

(14) Fenouillot, F.; Cassagnau, P.; Majesté, J.-C. Uneven Distribution of Nanoparticles in Immiscible Fluids: Morphology Development in Polymer Blends. *Polymer* **2009**, *50* (6), 1333–1350.

(15) Chung, H.; Ohno, K.; Fukuda, T.; Composto, R. J. Self-Regulated Structures in Nanocomposites by Directed Nanoparticle Assembly. *Nano Lett.* **2005**, *5* (10), 1878–1882.

(16) Walther, A.; Matussek, K.; Müller, A. H. E. Engineering Nanostructured Polymer Blends with Controlled Nanoparticle Location Using Janus Particles. *ACS Nano* **2008**, *2* (6), 1167–1178.

(17) Ruzette, A.-V.; Leibler, L. Block Copolymers in Tomorrow's Plastics. *Nat. Mater.* **2005**, *4* (1), 19–31.

(18) Kulasekere, R.; Kaiser, H.; Ankner, J. F.; Russell, T. P.; Brown, H. R.; Hawker, C. J.; Mayes, A. M. Homopolymer Interfaces Reinforced with Random Copolymers. *Macromolecules* **1996**, *29* (16), 5493–5496.

(19) Pieranski, P. Two-Dimensional Interfacial Colloidal Crystals. *Phys. Rev. Lett.* **1980**, *45* (7), 569–572.

(20) Kim, S.; Yoo, M.; Kang, N.; Moon, B.; Kim, B. J.; Choi, S.-H.; Kim, J. U.; Bang, J. Nanoporous Bicontinuous Structures via Addition of Thermally-Stable Amphiphilic Nanoparticles within Block Copolymer Templates. *ACS Appl. Mater. Interfaces* **2013**, *5* (12), 5659–5666.

(21) Yoo, M.; Kim, S.; Lim, J.; Kramer, E. J.; Hawker, C. J.; Kim, B. J.; Bang, J. Facile Synthesis of Thermally Stable Core−Shell Gold Nanoparticles via Photo-Cross-Linkable Polymeric Ligands. *Macromolecules* **2010**, *43* (7), 3570–3575.

(22) Verduzco, R.; Li, X.; Pesek, S. L.; Stein, G. E. Structure, Function, Self-Assembly, and Applications of Bottlebrush Copolymers. *Chem. Soc. Rev.* **2015**, *44* (8), 2405–2420.

(23) Paturej, J.; Sheiko, S. S.; Panyukov, S.; Rubinstein, M. Molecular Structure of Bottlebrush Polymers in Melts. *Sci. Adv.* **2016**, *2* (11), e1601478.

(24) Sheiko, S. S.; Zhou, J.; Arnold, J.; Neugebauer, D.; Matyjaszewski, K.; Tsitsilianis, C.; Tsukruk, V. V.; Carrillo, J.-M. Y.; Dobrynin, A. V.; Rubinstein, M. Perfect Mixing of Immiscible Macromolecules at Fluid Interfaces. *Nat. Mater.* **2013**, *12* (8), 735–740.

(25) Pesek, S. L.; Lin, Y.-H.; Mah, H. Z.; Kasper, W.; Chen, B.; Rohde, B. J.; Robertson, M. L.; Stein, G. E.; Verduzco, R. Synthesis of Bottlebrush Copolymers Based on Poly(Dimethylsiloxane) for Surface Active Additives. *Polymer*.

(26) Mitra, I.; Li, X.; Pesek, S. L.; Makarenko, B.; Lokitz, B. S.; Uhrig, D.; Ankner, J. F.; Verduzco, R.; Stein, G. E. Thin Film Phase Behavior of Bottlebrush/Linear Polymer Blends. *Macromolecules* **2014**, *47* (15), 5269–5276.

(27) Sun, F. C.; Dobrynin, A. V.; Shirvanyants, D.; Lee, H.-I.; Matyjaszewski, K.; Rubinstein, G. J.; Rubinstein, M.; Sheiko, S. S. Flory Theorem for Structurally Asymmetric Mixtures. *Phys. Rev. Lett.* **2007**, *99* (13), 137801.

(28) Wang, H. S.; Khan, A.; Choe, Y.; Huh, J.; Bang, J. Architectural Effects of Organic Nanoparticles on Block Copolymer Orientation. *Macromolecules* **2017**, *50* (13), 5025–5032.

(29) Sanford, M. S.; Love, J. A.; Grubbs, R. H. A Versatile Precursor for the Synthesis of New Ruthenium Olefin Metathesis Catalysts. *Organometallics* **2001**, *20* (25), 5314–5318.

(30) Mansky, P.; Liu, Y.; Huang, E.; Russell, T. P.; Hawker, C. Controlling Polymer-Surface Interactions with Random Copolymer Brushes. *Science* **1997**, *275* (5305), 1458–1460.

(31) Ahn, D. U.; Wang, Z.; Campbell, I. P.; Stoykovich, M. P.; Ding, Y. Morphological Evolution of Thin PS/PMMA Films: Effects of Surface Energy and Blend Composition. *Polymer* **2012**, *53* (19), 4187–4194.

(32) Mahadevapuram, N.; Mitra, I.; Bozhchenko, A.; Strzalka, J.; Stein, G. E. In-Plane and out-of-Plane Defectivity in Thin Films of Lamellar Block Copolymers. *J. Polym. Sci. Part B Polym. Phys.* **2016**, *54* (2), 339–352.

(33) Heriot, S. Y.; Jones, R. A. L. An Interfacial Instability in a Transient Wetting Layer Leads to Lateral Phase Separation in Thin Spin-Cast Polymer-Blend Films. *Nat. Mater.* **2005**, *4* (10), 782–786.

(34) Wu, S. Polar and Nonpolar Interactions in Adhesion. *J. Adhes.* **1973**, *5* (1), 39–55.

(35) Walheim, S.; Böltau, M.; Mlynek, J.; Krausch, G.; Steiner, U. Structure Formation via Polymer Demixing in Spin-Cast Films. *Macromolecules* **1997**, *30* (17), 4995–5003.

(36) Rubinstein, R. H., Michael, Colby. *Polymer Physics*; Oxford University Press, 2003.

(37) Li, X.; ShamsiJazeyi, H.; Pesek, S. L.; Agrawal, A.; Hammouda, B.; Verduzco, R. Thermoresponsive PNIPAAM Bottlebrush Polymers with Tailored Side-Chain Length and End-Group Structure. *Soft Matter* **2014**, *10* (12), 2008.

(38) Kohl, P. R.; Seifert, A. M.; Hellmann, G. P. Miscibility of Poly (Styrene-Co-Methylmethacrylate)s Differing in Composition. *J. Polym. Sci. Part B Polym. Phys.* **1990**, *28* (8), 1309–1326.

(39) Kulasekere, R.; Kaiser, H.; Ankner, J. F.; Russell, T. P.; Brown, H. R.; Hawker, C. J.; Mayes, A. M. Homopolymer Interfaces Reinforced with Random Copolymers. *Macromolecules* **1996**, *29* (16), 5493–5496.

(40) Trombly, D. M.; Ganesan, V. Curvature Effects upon Interactions of Polymer-Grafted Nanoparticles in Chemically Identical Polymer Matrices. *J. Chem. Phys.* **2010**, *133* (15), 154904.

(41) Wu, D. T.; Fredrickson, G. H. Effect of Architecture in the Surface Segregation of Polymer Blends. *Macromolecules* **1996**, *29* (24), 7919–7930.

(42) Walton, D. G.; Mayes, A. M. Entropically Driven Segregation in Blends of Branched and Linear Polymers. *Phys. Rev. E* **1996**, *54* (3), 2811–2815.

(43) Mezzenga, R.; Ruokolainen, J.; Fredrickson, G. H.; Kramer, E. J.; Moses, D.; Heeger, A. J.; Ikkala, O. Templating Organic Semiconductors via Self-Assembly of Polymer Colloids. *Science* **2003**, *299* (5614), 1872–1874.

(44) Shi, W.; Hamilton, A. L.; Delaney, K. T.; Fredrickson, G. H.; Kramer, E. J.; Ntaras, C.; Avgeropoulos, A.; Lynd, N. A.; Demassieux, Q.; Creton, C. Aperiodic “Bricks and Mortar” Mesophase: A New Equilibrium State of Soft Matter and Application as a Stiff Thermoplastic Elastomer. *Macromolecules* **2015**, *48* (15), 5378–5384.

606 Table of Contents Graphic

607

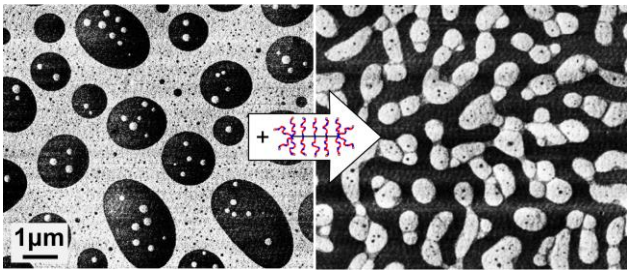

608